Journal of Renewable and Sustainable Energy

A new leakage detection method of molten salt tank and its experimental verification and optimization

Cite as: J. Renewable Sustainable Energy **14**, 043701 (2022); https://doi.org/10.1063/5.0093179
Submitted: 27 March 2022 • Accepted: 11 June 2022 • Published Online: 05 July 2022

Yuhang Zuo, Zhonghua Huang, Hui Zhao, et al.

Journal of Renewable and Sustainable Energy ARTICLE scitation.org/journal/rse

A new leakage detection method of molten salt tank and its experimental verification and optimization

Cite as: J. Renewable Sustainable Energy **14**, 043701 (2022); doi: 10.1063/5.0093179
Submitted: 27 March 2022 · Accepted: 11 June 2022 ·
Published Online: 5 July 2022

Yuhang Zuo,[1] Zhonghua Huang,[1,2] Hui Zhao,[2] Mingrui Zhang,[1] Fangzheng Cheng,[1] Hua Shi,[1] and Hao Zhou[1,a),b)]

AFFILIATIONS

[1]State Key Laboratory of Clean Energy Utilization, Institute for Thermal Power Engineering, Zhejiang University, Hangzhou 310027, China
[2]Shanghai Electric Power Generation Engineering Co., Shanghai 201199, China

[a)]**Permanent address:** State Key Laboratory of Clean Energy Utilization, Zhejiang University, Zheda Road 38, Hangzhou 310027, China.
[b)]**Author to whom correspondence should be addressed:** zhouhao@zju.edu.cn. **Tel.:** +86-0571-87952598

ABSTRACT

Molten salt tank leak detection technology is essential for the timely detection and handling of leaks. Current common thermocouple leak detection technology cannot meet the demand, and more efficient leak detection technology is urgently needed. In this paper, a molten salt tank leakage detection circuit based on the conductivity of high-temperature molten salt is proposed for the first time. Its feasibility is verified by the experimental results of a lab-scale tank foundation experimental system, and a parametric analysis is carried out to optimize the circuit layout. The results show that when molten salt leaks to the measurement point of the circuit, the voltage of the constant resistor in the circuit first rises rapidly, then drops rapidly, and finally, reaches a steady value. The vertical spacing, arrangement depth, and operating temperature significantly influence the detection effect. To ensure the rapid and continuous detection of molten salt tank leakage, the vertical spacing should be less than 50 mm. The arrangement depth should be as close as possible to the bottom of the molten salt tank, preferably within 150 mm. The decrease in the operating temperature significantly deteriorates the continuous detection effect of the circuit. When the detection circuit is used in the cold molten salt tank of concentrating solar power plants, timely circuit detection signal processing and prompt mechanisms are required to ensure that the leakage accident is not missed.

NOMENCLATURE

h	vertical spacing between the horizontal wire and the vertical wire (mm)
L_m	maximum migration depth (mm)
L_1	distance between the top of the solid molten salt block and the top of the fillers (mm)
L_2	length of the solid molten salt block (mm)
q	heat flux (W/m^2)
t	time (min)
T	temperature (°C)
T_{op}	operating temperature (°C)
U	voltage (V)
U_{max}	maximum voltage (V)
U_{steady}	steady voltage (V)
v_a	volume fraction of the air
W_m	maximum migration width (mm)
z	coordinate (mm)
λ_a	thermal conductivity of the air (W/m K)
λ_e	effective thermal conductivity (W/m K)
λ_f	thermal conductivity of the fillers (W/m K)

I. INTRODUCTION

Concentrating solar power (CSP) is one of the most promising renewable energy power generation technologies.[1,2] It is estimated that CSP will account for 11.3% of global power generation by 2050.[3] However, CSP also has inherent intermittent and volatility problems which brings challenges to its compatibility with the power grid. Integrating the thermal energy storage system (TESS) is an effective way to solve these problems and reduce the levelized cost of electricity (LCOE) of the CSP plant. By the end of 2017, 50.86% of the 116 CSP plants under construction or in operation worldwide were equipped with the TESS.[4] To meet the needs of CSP plants, the medium of the

TESS is required to have good transport and thermal properties. Based on that, molten salt is considered to be one of the best heat transfer/storage fluids of CSP plants.[5] Currently, the two-tank molten salt TESS is mainly adopted for CSP plants, and the most widely used molten salt is the solar salt composed of 60 wt. % $NaNO_3$ and 40 wt. % KNO_3.[6,7]

During the operation of the molten salt tank, heat will be dissipated to the surroundings and the tank foundation, and solar salt will solidify when the temperature is lower than about 220 °C. Thus, heat loss is critical to the safe and efficient operation of the molten salt tanks and the whole plant. Researchers have done a lot of work in this field.[8–17] Due to the large volume, large bottom area, high operating temperature of the medium, uneven temperature distribution in the tank, immature design and manufacturing technology, and cyclic charging/discharging process, the molten salt tank often suffers huge thermal stress, which may result in tank rupture and leakage accident after long-term use. Recently, the leakage accidents of the molten salt tanks in the Gemsolar plant and the Crescent Dune plant caused huge economic losses, and the prevention, detection, and treatment of molten salt tank leakage accidents have aroused people's attention.[18] To prevent the molten salt tank leakage, some researchers have explored the mechanical performance of the tank. Gauge *et al.*[19] evaluated the feasibility of chloride molten salt tank technology for the next generation CSP plant. With the assistance of the expansion joint design and finite element analysis software, the maximum stress of the tank shell was optimized to the allowable range. Wan *et al.*[4] conducted a simulation study on the mechanical performance of the hot tank of the two-tank molten salt TESS. The results showed that the maximum stress occurred on the inner corner between the tank bottom and the shell wall. The decrease in the molten salt level and the increase in the stiffness of the tank foundation fillers could decrease the stress. Wang *et al.*[20] conducted extensive parameter studies on the mechanical performance of a molten salt thermocline tank. The results showed that the increases in inlet velocity, cold salt temperature, and refractory brick thickness or the decreases in tank wall thickness, bed porosity, filler diameter, thermal conductivity, and specific heat could reduce the maximum mechanical stress of the tank wall. Once the molten salt tank leaks, the molten salt will migrate and solidify in the porous tank foundation material, and even pollute the soil and groundwater.[21] To better deal with the leakage accident, it is necessary to understand the leakage characteristics of molten salt in the tank foundation material. Some researchers have studied the migration or solidification characteristics of salt solutions in porous media. Song *et al.*[22] experimentally and theoretically studied the lateral freezing of the aqueous saline solution in porous medium and discussed the influence of the permeability of the porous matrix. Weisbrod *et al.*[23] studied the migration phenomenon and the mechanism of concentrated $NaNO_3$ solution in the uniform pre-wetted silica sand and found that solutions of 5 molal $NaNO_3$ migrated downward 24%–62% faster than pure water. Hird *et al.*[24] investigated the upward migration of saline (NaCl) fluid in the dry sand column and explored whether the salt transportation through the capillary phenomenon of fine sand was feasible. Dawson *et al.*[25] established a growth model of crystalline deposits from dripping salt solutions, and the calculated results of the model were pretty consistent with the experimental data. Other researchers studied the migration and solidification characteristics of molten salt in porous media. Shan *et al.*[26] studied the influence of leakage aperture, leakage temperature, and leakage velocity on the migration range of solar salt when it leaked to the soil surface based on the volume of fluid (VOF) model and continuous surface force (CSF) model, and the leakage characteristics of solar salt and SYSU-N1 salt were compared and analyzed. Wu *et al.*[27] and Zhang *et al.*[28] conducted experimental and numerical studies on the migration and solidification characteristics of molten salt in the cold soil porous system, revealing the influence of various operating and structural parameters on the molten salt migration range. The results showed that the increases of the inlet velocity, inlet temperature, soil porosity, or particle size increased the maximum migration depth. On this basis, to get closer to the actual molten salt tank leakage, Zhou *et al.*[21] built a thermal tank foundation experiment platform to investigate the influences of filler porosity, leakage aperture, operating temperature, and leakage mass on the migration and solidification characteristics of the molten salt in thermal stable porous materials and found that the greatest influencing factor was the operating temperature.

The leakage of a molten salt tank is usually a small-scale leakage in the early stage, but it will gradually spread and expand, and eventually become a large-scale leakage. Therefore, it is pretty critical to conduct early detection and treatment of the accidents to ensure the normal operation of CSP plants, avoiding the expansion and deterioration of leakage accidents. For liquid leak detection, there have been many studies. For example, for water tanks, the most common leak detection methods include volume and mass measurement, statistical inventory reconciliation, liquid sensor probes, and fiber-optic sensor probes.[29–31] The first two methods use the unexplainable mass loss to indicate the presence of a leak and cannot obtain the accurate location of the leak.[32] For molten salt tanks, the molten salt in the tank always undergoes the process of dynamic charging and discharging, and the volume and mass change all the time. Thus, these methods are difficult to cope with smaller leaks. Probe measurement uses probes to detect changes in the physicochemical signal after the liquid leaks, thereby providing accurate information about the leak. However, this method requires probes to be buried in advance. When the number of probes required for the storage tank is large, this method is costly, and the arrangement of a large number of probes may cause damage to the structure and characteristics of the tank foundation.[29] Unlike water tanks, the media in molten salt tanks have high temperature and strong corrosiveness, and most probe methods cannot be applied. At present, the CSP plant mainly detects the molten salt tank leakage by embedding a certain number of thermocouples in the tank foundation. However, due to the high cost, installation difficulty, and damage to the structure and heat dissipation of the tank foundation after installing the thermocouples, the number of embedded thermocouples is limited, resulting in a large detection area for a single thermocouple. Since the thermocouple is a point-type temperature measurement technology, this method cannot achieve good coverage of the tank foundation. In addition, the temperature of the tank foundation is also changing during the operation of the plant, and it is difficult to distinguish smaller leaks by the thermocouple method.

The leakage accidents of molten salt tanks are extremely detrimental to the normal operation and economic benefits of concentrating solar power plants, the leakage detection technology of molten salt tanks is critical to discover and deal with the leakage accidents promptly. Unfortunately, current research on molten salt tanks mainly focuses on temperature distribution and heat loss, mechanical

performance, migration and solidification characteristics after the tank leaks, and there is almost no research on leakage detection. The current common detection method with thermocouples is difficult to achieve good coverage of the entire tank foundation and to distinguish smaller leaks. To address the deficiencies of current leakage detection technology, a molten salt tank leakage detection circuit based on the conductivity of high-temperature molten salt was first proposed in this paper. Relevant experiments were carried out to verify its feasibility. In addition, the effects of vertical spacing, arrangement depth, and operating temperature on the detection effect were analyzed, and the beneficial results of optimizing the detection circuit layout were obtained. The proposed molten salt tank leakage detection method can reliably detect the leakage and has the advantages of low cost, simple installation, and little impact on the structure and heat dissipation characteristics of the tank foundation. It has a good prospect of large-scale commercial application and is of great significance to solve the problem of molten salt tank leakage detection.

II. LEAKAGE DETECTION CIRCUIT OF THE MOLTEN SALT TANK

Figure 1 shows the structure of the molten salt tank and tank foundation of a tower CSP plant. It is the load-bearing foundation below the molten salt tank of the CSP plant, which is usually composed of multiple layers of thermal insulation materials and the bottom concrete slabs. The load-bearing capacity of the foundation may decrease when the concrete slab overheats or the moisture of the tank foundation evaporates, so the concrete slab is usually equipped with ventilation pipes to accelerate heat dissipation.[4,33] In actual operation, the thermal stress of the bottom plate and the intersection of the bottom plate and the side shell are relatively large, so the molten salt tank leakage usually occurs in these positions. After the molten salt tank leaks, the molten salt will flow from the tank bottom into the insulation material of the tank foundation. To detect the molten salt tank leakage of the CSP plant, we propose a detection circuit based on the conductivity of the high-temperature molten salt. As shown in Fig. 2, the detection circuit including the three-dimensional wire group is embedded in the thermal insulation material of the tank foundation. The three-dimensional wire group consists of the horizontal parallel wire group and the longitudinal parallel wire group, and the horizontal parallel wire group and the longitudinal parallel wire group are arranged at different depths of the tank foundation. The material of the wires is 347H stainless steel with good conductivity, high-temperature resistance, and molten salt corrosion resistance. The three-dimensional wire group is connected in series with the first constant resistors and second constant resistors, and the first constant resistors and second constant resistors are, respectively, connected to the positive and negative electrodes of the direct current (DC) power supply. As a result, a molten salt leak detection circuit with multiple detection loops is formed, wherein each of the first constant resistors and second constant resistors has the same resistance. During the operation, the DC power supply is turned on, and the electrical signals of all the first constant resistors and second constant resistors are recorded by different channels of the data acquisition and alarm device. Once the corresponding channel monitors the electrical signal, the corresponding alarm device quickly alarms to remind the leakage accident of the molten salt tank.

In the detection circuit, the horizontal parallel wire group and the longitudinal parallel wire group are not in contact, then many measuring points are formed in the tank foundation. Initially, there is no electrical signal in each recording channel due to the disconnection of the circuit. When the molten salt leaks to any measuring point, due to the electrical conductivity of the high-temperature molten salt, the electrical signals of the first constant resistor and the second constant resistor change rapidly to realize the rapid detection and accurate positioning of the molten salt tank leakage. The determination of the leakage location of the molten salt tank is carried out in the following three steps. (1) When the electrical signal of any first constant resistor appears, the x coordinate of the measuring point where molten salt leakage is detected can be determined. (2) According to the electrical signal of the second constant resistor, the y coordinate of the measuring point where molten salt leakage is detected can be determined. (3) Finally, the location of the measuring point where molten salt leakage is detected can be determined, and the location of molten salt tank leakage is usually near directly above the measuring point. To ensure reliable, efficient, and comprehensive detection, the number of wires in the three-dimensional wire group can be selected according to the actual molten salt tank size to make the entire tank bottom is covered.

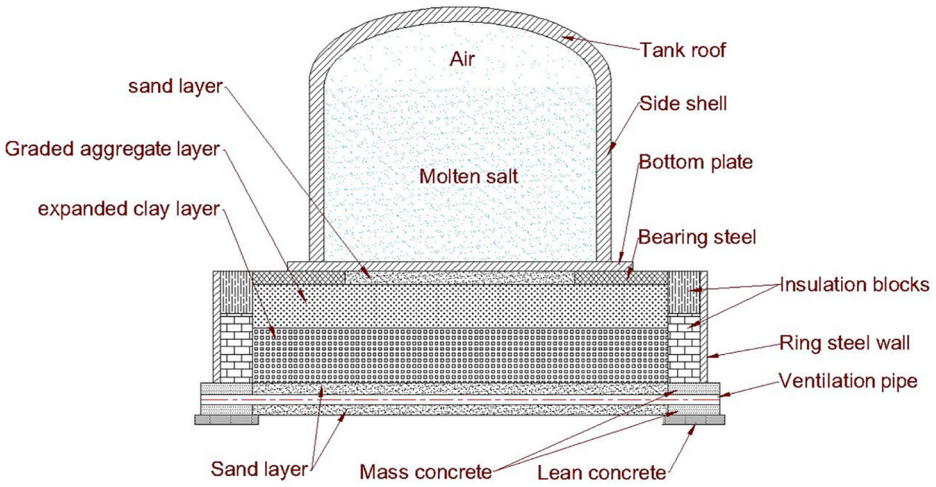

FIG. 1. Structure of the molten salt tank and tank foundation of a tower CSP plant.

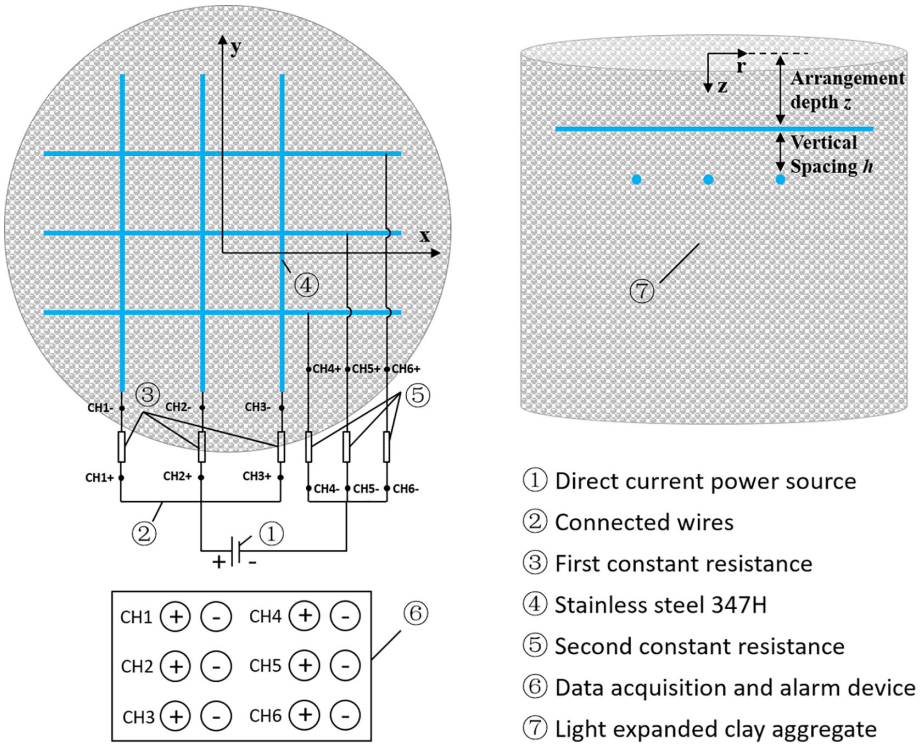

FIG. 2. Schematic diagram of the leakage detection circuit of the molten salt tank based on high temperature molten salt conductivity.

III. EXPERIMENTAL SETUP AND METHOD

A. Experimental setup and materials

To verify the feasibility of the proposed molten salt tank leakage detection method and optimize the detection circuit layout, a lab-scale experimental system of molten salt tank foundation is built. As shown in Fig. 3, the diameter and height of the inner hole of the tank are 1000 and 900 mm, respectively. The light expanded clay aggregate (LECA) is widely used as a thermal insulation material for molten salt tank foundations in the actual CSP plant due to its low cost, light weight, and good load-bearing and thermal insulation performance.[33] Thus, the LECAs with mixed particle sizes are used as the fillers. The mixed LECAs are shown in Fig. 4, and the particle size distribution, bulk density, and porosity are shown in Table I. A programmable resistance heater is installed below the tank cover plate. The function of the heater is to heat the fillers from the top, so as to restore the temperature distribution of the tank foundation of the actual CSP plant. In addition, the upper part of the cover plate is connected with a pulley, so that it can be lifted or lowered during the experiment. The refractory brick with a thickness of 250 mm is used in the sidewall of the tank to reduce the heat dissipation of fillers to the surroundings. The molten salt leaking into the fillers will eventually form the solid molten salt block (SMSB) after cooling. To remove the SMSB smoothly, the bottom plate of the tank is designed to be openable. Fifteen K-type thermocouples with a uniform longitudinal spacing of 50 mm are installed on the sidewall of the tank to measure the temperatures of the fillers during the experiment, and the temperature measurement accuracy of the thermocouple is ±0.75%. The top thermocouple was 50 mm away from the top of the fillers, and the temperature measuring terminal of each thermocouple is inserted into the center of the tank. The temperatures measured by thermocouples are recorded by the Agilent data acquisition device, which measures temperature and DC voltage with an accuracy of ±1.0 °C and ±0.004%, respectively. Finally, to obtain high-temperature molten salt, the muffle furnace with an accuracy of ±1.0 °C is used for melting and heating of molten salt. The molten salt used in this paper is a solar salt, and its properties are shown in Table II.[21]

B. Experimental method of leak detection

To verify the feasibility of the leakage detection circuit and optimize its layout, we designed the simplified detection circuit shown in Fig. 5 for the experimental study. The simplified leakage detection circuit is only arranged in the center of the fillers, including one longitudinal wire and five horizontal wires. The longitudinal wire is connected to the positive pole of the 3 V DC power supply and arranged above the horizontal parallel wire group. The five horizontal parallel wires are only 25 mm apart from each other, and they are, respectively, connected to a 1000 Ω constant resistor, and the other end of each constant resistor is connected to the negative pole of the DC power supply. The constant resistors are connected to different channels of the Agilent data acquisition device to record the voltage signals. The reason for arranging five horizontal wires is to prevent the molten salt leakage position from deviating from the center in the experiment, so that the voltage signal can always be measured. While analyzing the data, only the channel with the largest signal among the five channels is selected. The horizontal and longitudinal wires in the experimental circuit

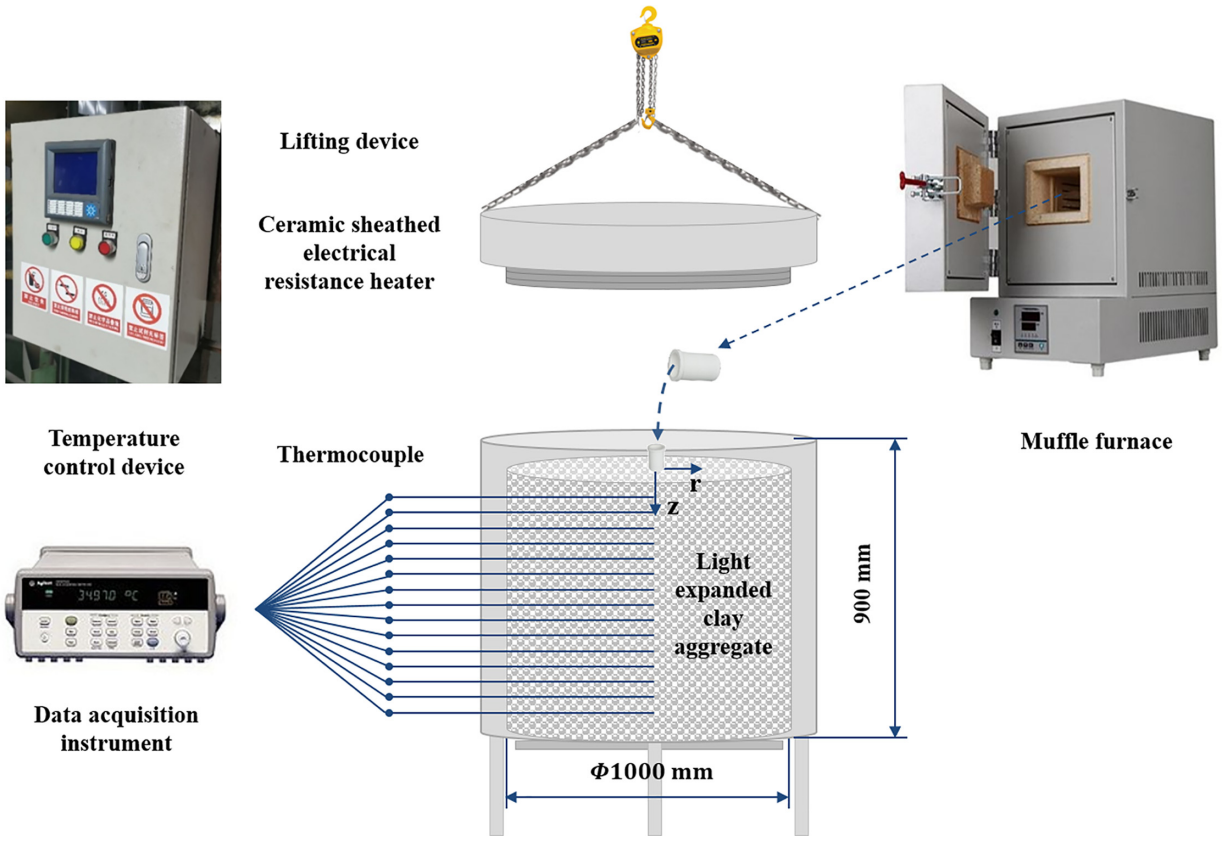

FIG. 3. Schematic diagram of the experimental system.

FIG. 4. The appearance of the experimental material (LECAs) with mixed particle size.

TABLE I. Properties of the LECA.

Properties	Value
Particle size distribution	3.35–6.3 mm 39% 6.3–8 mm 31% 8–10 mm 13% 10–20 mm 17%
Bulk density (kg/m^3)	596.73
Porosity (%)	35.8

TABLE II. Properties of solar salt.

Properties	Formulas
Density (kg/m^3)	$2263.7–0.636\times T$
Specific heat (J/kg K)	$1396+0.172\times T$
Thermal conductivity (W/m K)	$0.391+0.000\,19\times T$
Dynamic viscosity (Pa s)	$0.0755–2.776\times10^{-4}\times T$ $+3.489\times10^{-7}\times T^2$ $-1.474\times10^{-10}\times T^3$

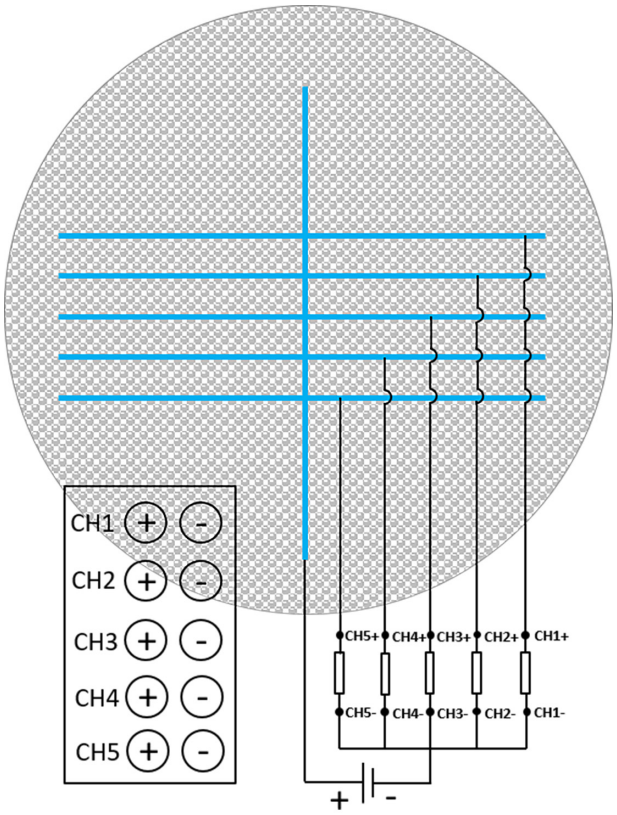

FIG. 5. Molten salt leakage detection circuit used in experiment.

are 347H steel bars with a diameter of 5 mm and a length of 330 mm. The experimental conditions are shown in Table III.

The experimental process is divided into three stages: filler heating, molten salt leakage, and filler cooling and post-treatment. At the filler heating stage, after the mixed LECAs are filled to a position 50 mm from the tank top, the tank cover plate is lowered. The programmable resistance heater with a predetermined temperature is then turned on, and the fillers are gradually heated to a stable state. At the same time, 600 g solar salt is weighed by the electronic balance with an accuracy of ± 0.1 g and put into the crucible. Then, the crucible containing molten salt and a crucible with a circular hole of 15 mm diameter at the bottom are both put into the muffle furnace and heated to the same predetermined temperature as the programmable resistance heater. The molten salt leakage begins after the temperature distribution of the fillers is stable. First, the cover plate is pulled up. Second, the crucible with a circular hole is taken out from the muffle furnace and placed in the center above the fillers, and then the high-temperature molten salt is taken out and poured into the fillers through the circular hole of the crucible. Finally, the cover plate is quickly lowered, and the heater continues to heat the fillers until the temperature stabilizes again. At this stage, the molten salt undergoes complex migration and phase change in the fillers. At the filler cooling and post-treatment stage, the heater is turned off, and the fillers gradually cool to ambient temperature. After that, the solid molten salt block is taken out, and its migration range is measured

TABLE III. Experimental conditions.

Case	Operating temperature (°C)	Vertical spacing (vertical spacing between horizontal wire and longitudinal wire) (mm)	Arrangement depth (vertical distance between horizontal wire and the top of fillers) (mm)
A1	565	20	100
A2	565	50	100
A3	565	80	100
A4	565	110	120
B1	565	50	150
B2	565	50	200
B3	565	50	250
C1	290	50	100
C2	390	50	100
C3	500	50	100

by a tape with an accuracy of ±0.5 mm. The thermocouples and leakage detection circuit completely record the temperature and voltage signals in the whole experimental process.

To ensure the feasibility of the detection method, we first use the experimental system to test the electrical conductivity of the molten salt and fillers. Figure 6 shows the voltage evolution of the constant resistor with the temperature of the junction of the circuit (connected by the molten salt or the fillers). It can be seen that when the temperature is about 530 °C, the voltage is almost equal to the voltage of the DC power supply. As the molten salt temperature decreases, the voltage gradually decreases. When the temperature decreases near the melting point of the molten salt, the voltage decreases rapidly to near zero for the solidification of the molten salt and remains zero when the temperature continues to decrease. That is, the conductivity of the

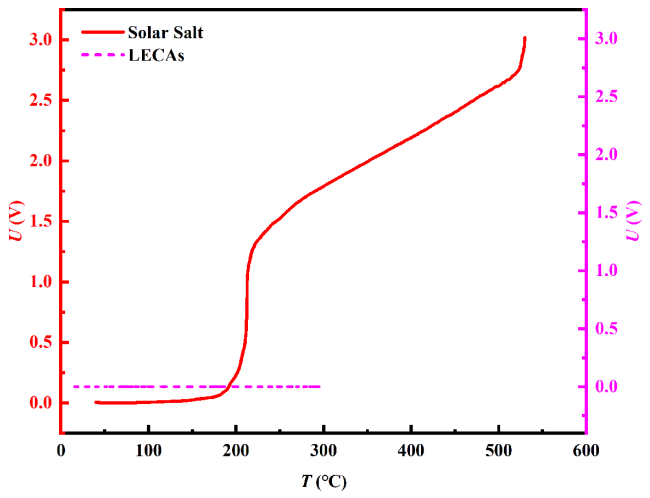

FIG. 6. Evolution of electrical conductivity of solar salt and LECAs with temperature.

solar salt increases with temperature, and it is not conductive in solid state. The above results are consistent with the theoretical situation. The solar salt is composed of two ionic compounds: $NaNO_3$ and KNO_3. In the molten state, there are freely movable ions inside the molten salt, so it is conductive. The higher the temperature, the faster the movement rate of internal ions, resulting in an increase in electrical conductivity. In the solid state, the ions cannot move freely, so it is not conductive. The electrical conductivity data of the fillers are obtained from the experimental results of the heating process of case A1. During the whole heating process, the voltage of the constant resistor remains zero, which indicates that the fillers are not conductive. The above results lay a good foundation for the feasibility of the proposed leakage detection circuit.

IV. RESULTS AND DISCUSSION

A. Temperature distribution and evolution characteristics

Figure 7 presents the temperature distribution and evolution of the fillers during the experiment at $T_{op} = 565\,^{\circ}C$. During the heating process, the temperature of the fillers increases gradually until reaching a steady state. Because the heater is on the top of the fillers, so the closer to the top, the faster the temperature rises and the higher the steady temperature is. The steady temperature at $z = 50$ mm is 467.1 °C, and the temperature distribution of the tank foundation is steady after about 40 h. During the molten salt leakage process, due to the heat exchange between the fillers and the high-temperature molten salt, the temperature of the area contacting with the high-temperature molten salt increases rapidly in succession and then decreases gradually after the high-temperature molten salt leaves. Since the temperature of the fillers gradually decreases from the top to the bottom, the temperature of the molten salt will drop below the melting point after migrating a certain distance and begin to solidify. The solidified molten salt is bonded with the fillers to form the SMSB, which hinders the continuous downward flow of the molten salt, so that the molten salt will gradually solidify upward from there.[28] Therefore, the flow of the molten salt in the fillers will stop finally, and a new steady temperature distribution will be formed. This process takes about 20 h. As for the cooling process, due to the stop of heating and the opening of the

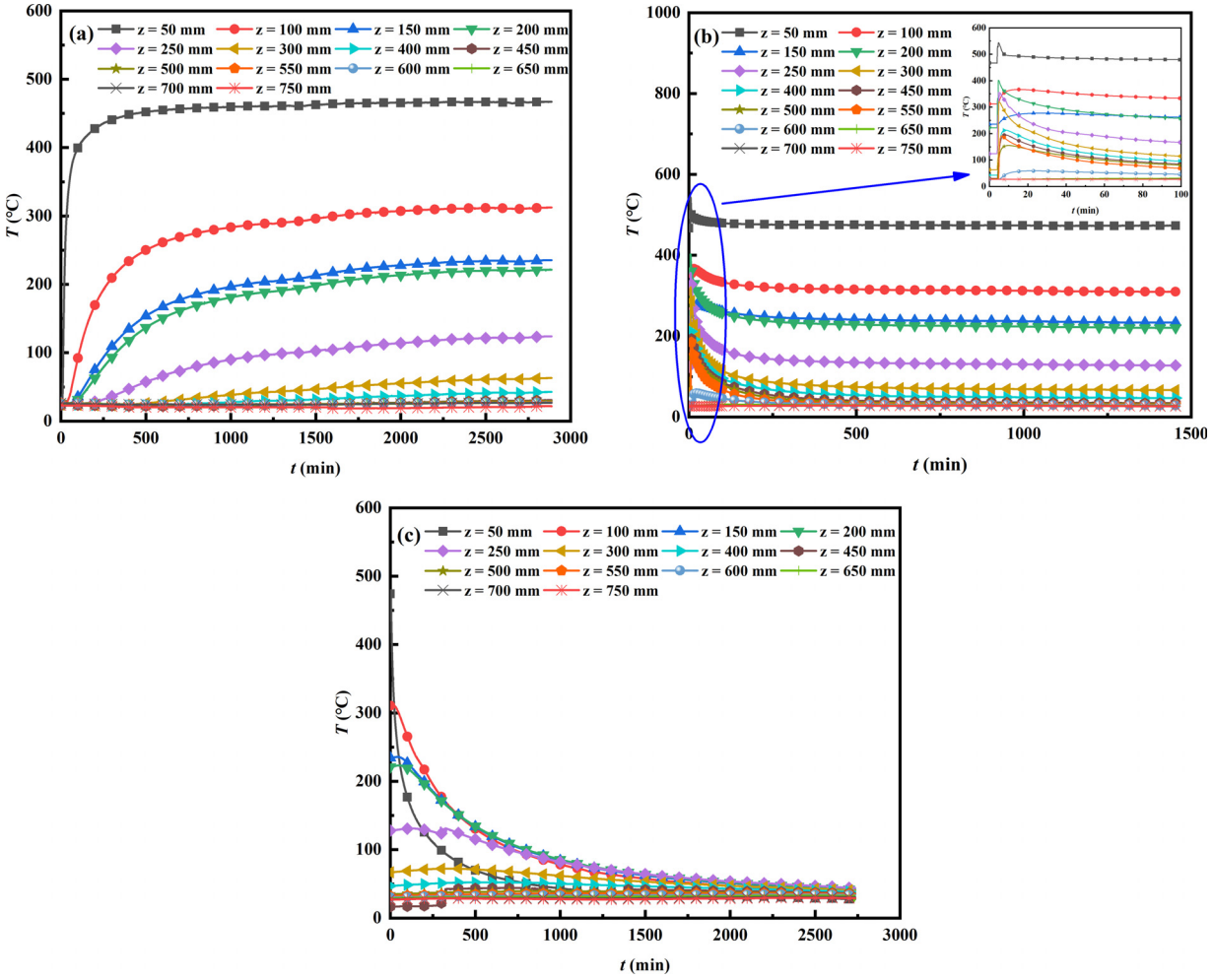

FIG. 7. Temperature distribution and evolution of the fillers during the experiment of case B3. (a) Heating process; (b) leakage process; and (c) cooling process.

cover plate, the temperature of the fillers eventually decreases to the ambient temperature, and the temperature in the upper part of the fillers decreases significantly faster. The cooling process takes about 40 h.

Figure 8 presents the steady-state temperature distribution when the heating process reaches stability at different operating temperatures. In the region of $z < 400$ mm, the steady temperature increases significantly with the increase in the operating temperature, while in the region of $z > 400$ mm, the change of operating temperature has only little influence on the temperature distribution. This is because that the lower part receives less heat and has a large heat dissipation. When the operating temperature is 290, 390, 500, and 565 °C, the steady temperature at $z = 50$ mm is 211.7, 284.8, 343.7, and 467.1 °C, respectively. In addition, because the heat dissipation of the upper part is large, the temperature gradient of the area closer to the top is larger, and the temperature gradient increases with the increase in the operating temperature.

The temperature evolution at $z = 50$ mm throughout the experiment at different operating temperatures is shown in Fig. 9. It can be noted that the steady temperature of the molten salt leakage process is higher than that of the heating process, and the difference increases with the increase in the operating temperature. For example, when the operating temperature increases from 290 to 565 °C, the difference increases from 1.2 to 6.3 °C. The above phenomenon is caused by the increase in the thermal conductivity of the filler area with molten salt after it leaks into the fillers. According to Fourier heat conduction law, for multilayer wall heat conduction, the heat flux can be expressed as

$$q = \frac{1 - T_{n+1}}{\sum_{i=1}^{n} \frac{\delta_i}{\lambda_i}}, \tag{1}$$

where q is the heat flux (W/m^2), T_1 and T_{n+1} are the temperatures of both ends of the multilayer wall (K), δ_i is the thickness of the layer i (m), and λ_i is the thermal conductivity of the layer i (W/m K).

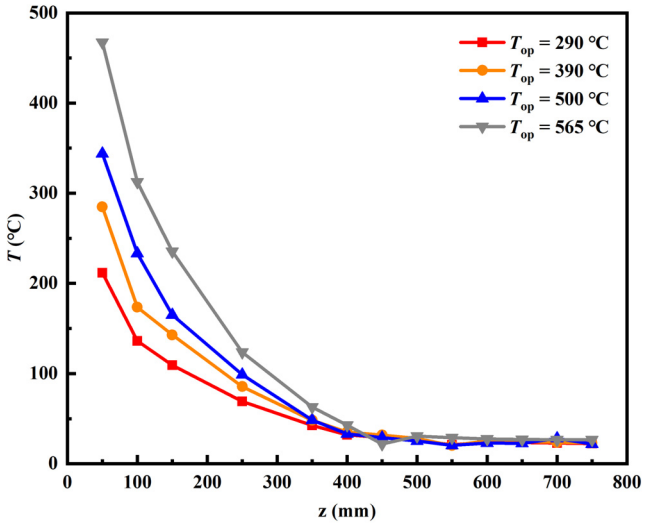

FIG. 8. Steady-state temperature distribution when the heating process reaches stability at different operating temperatures.

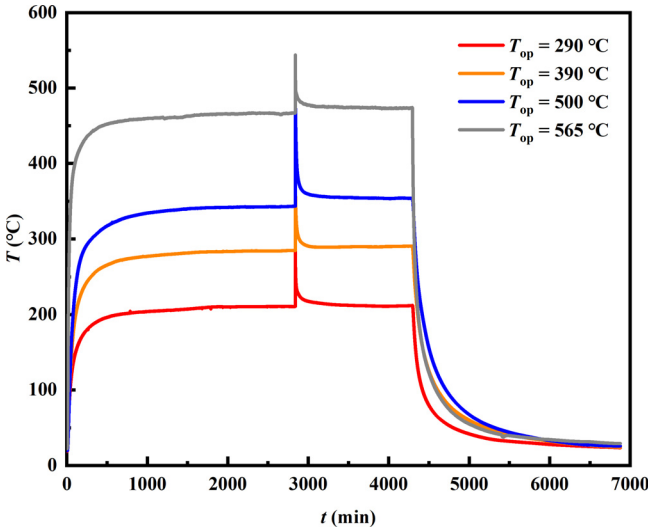

FIG. 9. Temperature evolution at $z = 50$ mm throughout the experiment at different operating temperatures.

For each layer of material, the heat flux can be expressed as

$$q = \lambda_i \frac{T_i - T_{i+1}}{\delta_i}. \tag{2}$$

Considering that the filler in this paper is the porous medium, the thermal conductivity in Eqs. (1) and (2) can be represented by the effective thermal conductivity of the porous medium. The effective thermal conductivity can be modeled by the equivalent medium theory (EMT) equation as follows:[34]

$$(1 - \nu_a)\frac{\lambda_f - \lambda_e}{\lambda_f + 2\lambda_e} + \nu_a \frac{\lambda_a - \lambda_e}{\lambda_a + 2\lambda_e} = 0. \tag{3}$$

Thus, λ_e can be written as follows:

$$\lambda_e = 1/4\Big((3\nu_a - 1)\lambda_a + [3(1 - \nu_a) - 1]\lambda_f + \sqrt{[(3\nu_a - 1)\lambda_a + [3(1 - \nu_a) - 1]\lambda_f]^2 + 8\lambda_f\lambda_a}\Big), \tag{4}$$

where λ_e, λ_f, and λ_a are, respectively, the effective thermal conductivity, thermal conductivity of the fillers, and thermal conductivity of the air, W/m K. ν_a is the volume fraction of the air.

The thermal conductivity of the molten salt is significantly higher than that of air. After the molten salt leaks into the fillers, the molten salt replaces part of the air in the upper part of the fillers. According to Eq. (4), it can be simply regarded as an increase in λ_a, so λ_e of the upper part of the fillers increases. Considering that the top of the fillers is in contact with the heater, the temperature there does not change after the molten salt leakage. The temperature at the bottom of the fillers is hardly affected by the molten salt leakage, so it also remains unchanged after the molten salt leakage. Since the overall effective thermal conductivity of the fillers increases, the heat flux q increases according to Eq. (1). The effective thermal conductivity of the lower part of the fillers where there is no molten salt remains unchanged after the molten salt

leakage. According to Eq. (2), the increase in heat flux will cause the temperature gradient at the lower part of the fillers to increase, so the temperature gradient at the upper part of the fillers decreases. As a result, in the filler area with the molten salt after the molten salt leakage, the steady-state temperature will be higher than that before the molten salt leakage. In addition, the higher the operating temperature, the greater the increase in λ_e and the greater the temperature rise.

B. Migration and phase change characteristics

The migration and phase change characteristics after the molten salt leakage are critical for understanding and handling the leakage accident of the molten salt tank. Figure 10 shows the final state after the molten salt leaks into the fillers. Several parameters are defined to describe the migration characteristics, including the distance between the top of the SMSB and the top of the fillers L_1, the length of the SMSB L_2, the maximum migration depth L_m, and the maximum migration width W_m. Figure 11 shows the migration results of the molten salt in the tank foundation materials after its leakage under different operating temperatures. The increase in the operating temperature means the higher temperatures of the molten salt and the fillers, which cause the maximum migration depth of the molten salt to increase significantly. The maximum migration depths at $T_{op} = 565$ and $T_{op} = 290\,^{\circ}\mathrm{C}$ are 702 and 355 mm, respectively. The former is almost twice that of the latter. Thus, it is especially important to prevent the leakage of the hot tank of the two-tank molten salt TESS. After the molten salt leaks into the fillers and migrates for a certain distance, its temperature will drop below its melting point. From there, the molten salt begins to solidify gradually. In the upper area of this position, only a small amount of molten salt remains after the leakage process is over, so the solid molten salt block will not form in this area after cooling. As the operating temperature rises, the position where the molten salt temperature drops below its melting point moves down. Thus, L_1 increases. When the operating temperature is 290, 390, and 565 °C, L_1 is 20, 120, and 300 mm, respectively. Considering that the temperature at the lower part of the fillers is less affected by the operating temperature, L_2 increases first and then decreases with the operating temperature. When the operating temperature is 290, 390, and 565 °C, L_2 is 335, 445, and 402 mm, respectively. The increase in operating temperature leads to an increase in L_m, while the amount of the leaking molten salt is constant, so W_m decreases as the operating temperature increases. When the operating temperature is 290, 390, and 565 °C, W_m is 134, 131, and 124 mm, respectively. The above results of the maximum migration depth and maximum migration width are consistent with the results of published literatures.[21,27,28]

To explain the morphological change of the SMSB, we proposed the solidification agglomeration model shown in Fig. 12. The entire fillers can be divided into the non-solidification zone, main solidification zone, second solidification zone, and no molten salt zone. As mentioned earlier, in the non-solidification zone, the molten salt does not agglomerate due to the small amount. The molten salt begins to solidify after it crosses the upper boundary of the main solidification zone. The lower boundary of the main solidification zone is the location where the molten salt concentrates and agglomerates here. After the solidification and concentration, only a small amount of molten salt can cross this position and enter the second solidification zone. As the molten salt solidifies and concentrates, the flow of molten salt above the position is hindered, so the molten salt gradually solidifies upward from here. When the operating temperature increases, the amount of molten salt passing through the main solidification zone increases, so that more molten salt solidifies in the second solidification zone. The lengths of the main solidification zone and the second solidification zone are variable. As the operating temperature increases, the solidification concentration position moves downward, leading to a longer main solidification zone and a downward movement of the second solidification zone. As shown in Fig. 13, the SMSB shows an obvious shape with a thin upper part and a thick lower part at $T_{op} = 290\,^{\circ}\mathrm{C}$. This is because it is difficult for molten salt to pass through the solidification concentration position. When the operating temperature increases to 390 °C, the molten salt passing through the

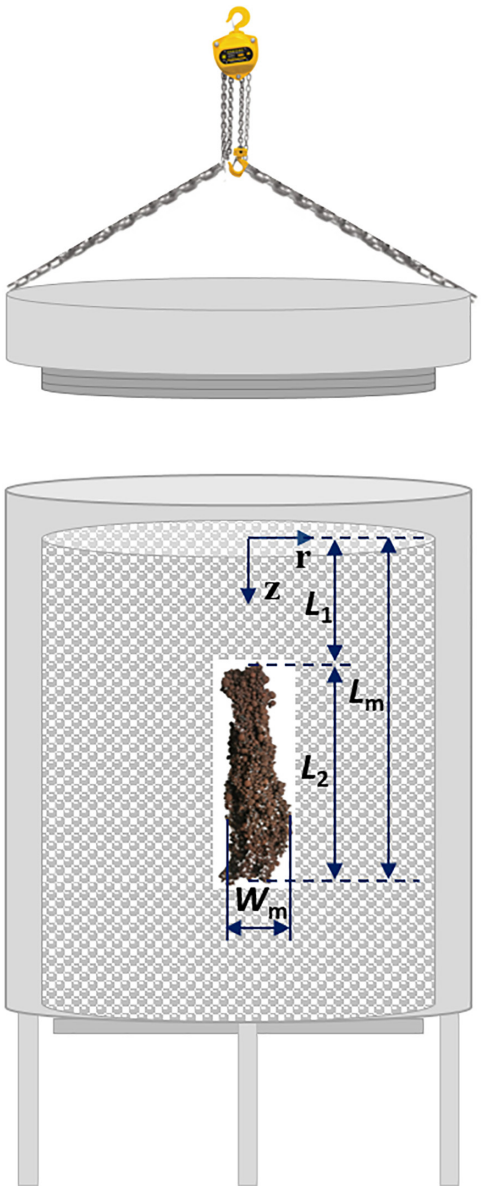

FIG. 10. Schematic diagram of the solidification molten salt block finally formed in the fillers after molten salt leakage.

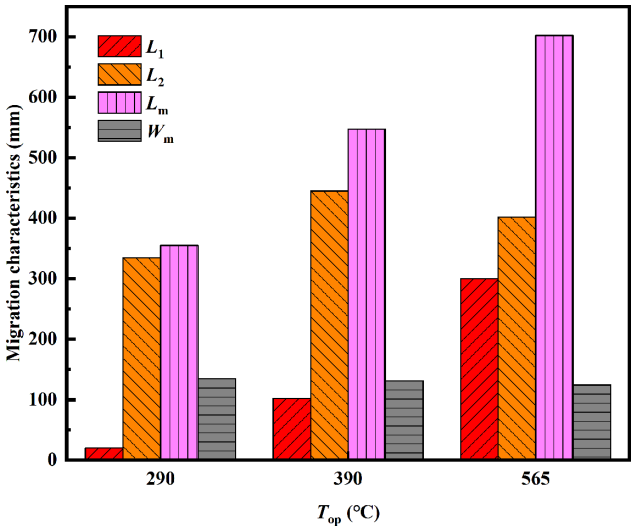

FIG. 11. Migration characteristics of molten salt leakage into tank foundation materials at different operating temperatures.

solidification concentration position increases, and a sharp tip appears at the bottom of the SMSB, and the upper part of the tip still presents the shape with a thin upper part and a thick lower part, though the width decreases. When the operating temperature further increases to 565 °C, the molten salt passing through the solidification concentration position increased significantly, and the width of the agglomeration at the bottom of the main solidification zone is close to that of the secondary solidification zone, so the SMSB returns to the shape of a thin upper part and a thick lower part.

C. Feasibility and parameter analysis of leak detection circuit

1. Typical voltage evolution

Among all the detection results, the voltage signal of the constant resistor shows the two patterns in Fig. 14. When the detection circuit

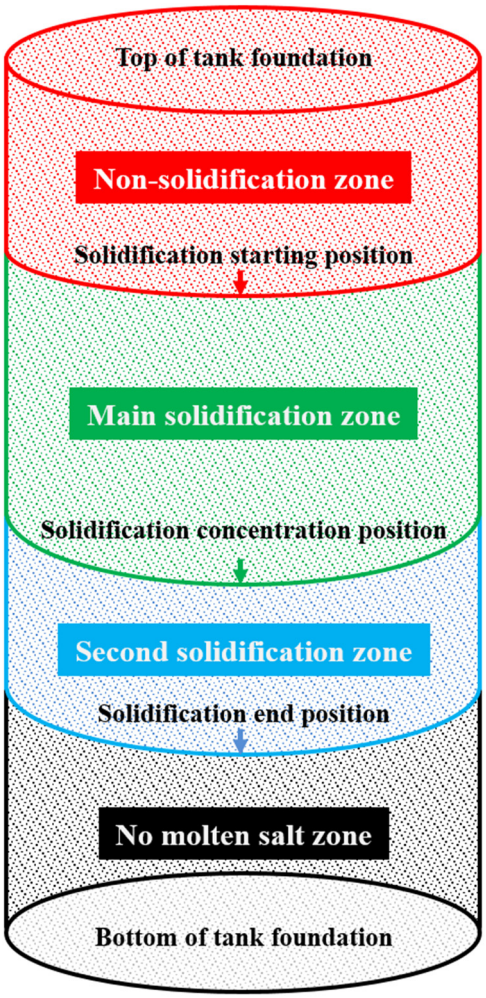

FIG. 12. Solidification agglomeration model after molten salt leaks into the tank foundation.

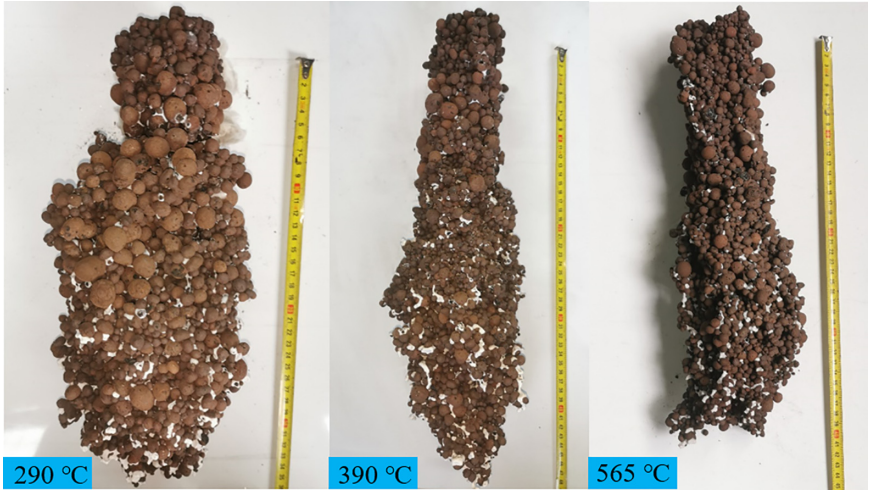

FIG. 13. Solid molten salt block formed after molten salt leaks into the tank foundation at different operating temperatures.

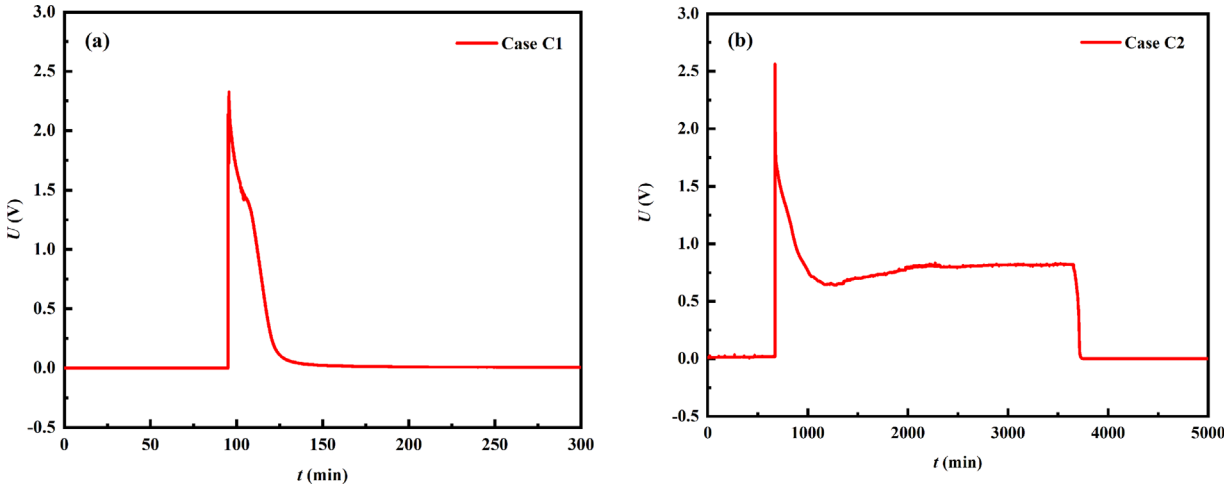

FIG. 14. Two typical situations of voltage evolution of constant resistor constant. (a) Typical situation 1 and (b) typical situation 2.

is arranged at a lower position or the operating temperature is lower (Cases B2, B3, and C1), the evolution of the voltage is shown in Fig. 14(a). During the heating process, the voltage is zero because the measuring point of the detection circuit is disconnected. After the molten salt leaks, the circuit is connected when the high-temperature molten salt migrates to the measuring point, and the voltage rises rapidly to the peak value. Because the measuring point is arranged at a lower position or the operating temperature is lower, when the molten salt continues to migrate downward, the amount and temperature of the molten salt in the connecting part of the measuring point decrease, or even the molten salt solidifies here, which makes the molten salt of the measuring point gradually lose conductivity. As a result, the voltage drops rapidly to zero and remains zero during the cooling process. When the detection circuit is arranged at a relatively high position or the operating temperature is high (Cases A1, A2, A3, A4, B1, C2, and C3), the evolution of the voltage is shown in Fig. 14(b). Compared with Fig. 14(a), the voltage in Fig. 14(b) will not drop to zero during the leakage process. This is because the temperature in the connecting part of the measuring point is higher, so that there is always conductive molten salt after the leakage. Since the amount and temperature of the molten salt at the measuring point gradually decrease, the conductivity of the molten salt also gradually decreases, and the voltage at the end of the leakage process is lower than the initial voltage. After the cooling process starts, the molten salt rapidly drops in temperature and solidifies, so the voltage rapidly drops to zero and then remains zero. Under all experimental conditions, the detection circuit has detected the leakage of the molten salt. Therefore, the proposed molten salt leakage detection method has good feasibility.

2. Parameter analysis

Figure 15 presents the voltage evolution of the constant resistor under different vertical spacings within 1000 min after the leakage. When the interval is less than 50 mm, the circuit can be quickly connected after the molten salt leaks, so the voltage rapidly reaches the peak value. However, once the interval exceeds 50 mm, although the voltage also appears quickly, the time to reach the peak value becomes significantly longer. When the interval is 20, 50, 80, and 110 mm, the time from the start of the leakage to the peak voltage is 0.05, 0.13, 46.6, and 139.3 min, respectively. Figure 16 presents the maximum voltage after the leakage and the steady voltage after 1000 min of the leakage under different longitudinal intervals. The maximum voltage and the steady voltage hardly change with the interval when the interval is less than 50 mm. This is mainly due to the small difference in the resistance of the connected part of the measuring point after the leakage within this interval. With the further increase in the interval, the resistance of the connected part changes with time due to the flow of the molten salt, and it takes a longer time to reach the maximum conductivity. As the interval increases, the resistance of the connected part also increases significantly, so the peak voltage and steady voltage decrease. Based on the above discussion, to ensure the rapidity and

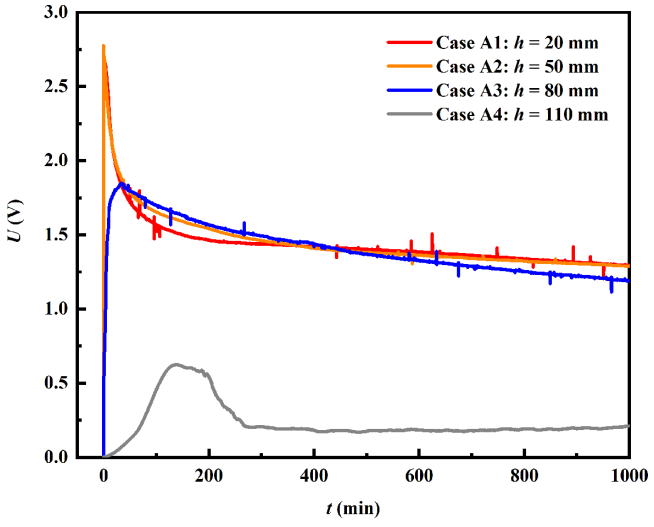

FIG. 15. Voltage evolution of measuring point at different vertical spacings (T_{op} = 565 °C, z = 100 mm for Cases A1, A2, and A3, and z = 120 mm for Case A4).

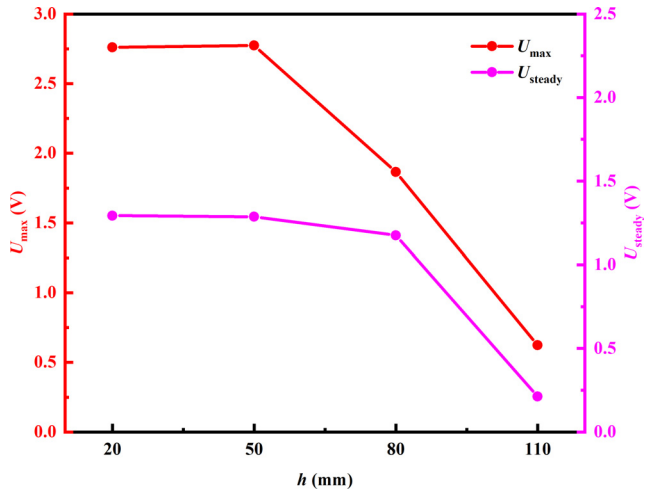

FIG. 16. The effect of vertical spacing on the maximum voltage and steady voltage (T_{op} = 565 °C, z = 100 mm for Cases A1, A2, and A3, and z = 120 mm for Case A4).

continuous effectiveness of the detection, the longitudinal interval between the horizontal wires and the longitudinal wires should not be too large, preferably less than 50 mm.

Figure 17 presents the voltage evolution of the constant resistor under different arrangement depths within 1000 min after the leakage. When the arrangement depth is z = 100, z = 150, z = 200, and z = 250 mm, the time from the start of the leakage to the peak voltage is 0.13, 2.35, 0.60, and 0.07 min, respectively. This time is directly related to the flow velocity of molten salt in the fillers. It can be noticed that this time is not the maximum when the arrangement depth is maximum. Due to the difference in the packing arrangement and the initial velocity of molten salt entering the fillers, the flow velocity of molten salt in the fillers is not consistent in each experimental condition, so it cannot be guaranteed that the greater the arrangement depth, the longer the time.

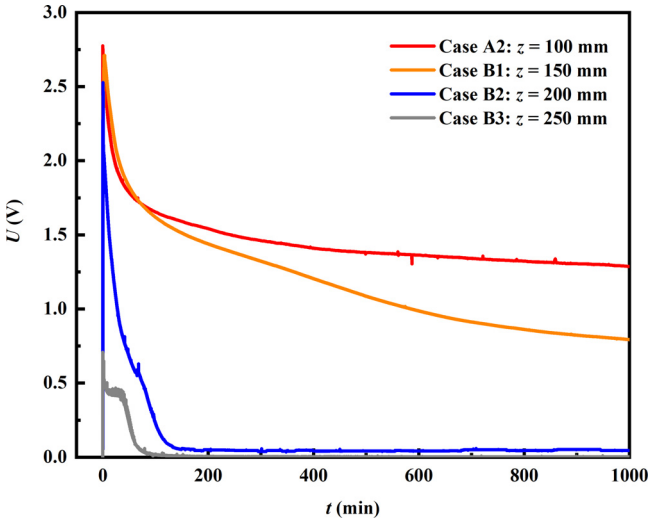

FIG. 17. Voltage evolution of the measuring point at different arrangement depths (T_{op} = 565 °C, h = 50 mm).

Overall, the arrangement depth has little influence on the detection speed within these arrangement depths. However, the arrangement depth greatly influences the maximum voltage and steady voltage. As shown in Fig. 18, as the arrangement depth increases, the temperature of the molten salt when it connects the circuit is lower, that is, the conductivity is lower, so the maximum voltage and steady voltage both decrease as the arrangement depth increases. For example, the maximum voltage and steady voltage at z = 250 mm are only 25.5% and 0.16% of those at z = 100 mm, respectively. Moreover, when the arrangement depth moves down, the period that the circuit can detect the leakage also be shortened. When the arrangement depth is z = 200 mm and above, the circuit can detect the leakage during the entire process. While the voltage is almost zero after only 125 min when the arrangement depth moves down to z = 250 mm. Therefore, an excessively large arrangement depth is not conducive to continuous detection of molten salt leakage and may lead to missed judgment of leakage accidents. Thus, the detection circuit should be arranged as close as possible to the tank bottom, preferably within 150 mm from the tank bottom.

For tower CSP plants, the molten salt temperatures in the cold tank and hot tank are usually 290 and 565 °C, respectively. Therefore, it is very important to study the influence of the operating temperature on the detection effect of the detection circuit. Figure 19 presents the voltage evolution of the constant resistor under different operating temperatures within 1000 min after the leakage. When the operating temperature is 290, 390, 500, and 565 °C, the time from the start of the leakage to the peak voltage is 0.03, 0.03, 0.08, and 0.13 min, respectively. So the operating temperature also has little effect on the detection speed. As shown in Fig. 20, the approximately linear positive correlation between the maximum voltage, the steady voltage, and the operating temperature can be noted, which is mainly caused by the change of the conductivity of the molten salt with temperature. The higher operating temperature is more conducive to the leakage detection. When the operating temperature is 290 °C, the voltage will quickly drop to zero after reaching the peak value, which results in a shorter period for the circuit to detect the leakage. Therefore, if the proposed leakage detection circuit is applied to the cold tank of the

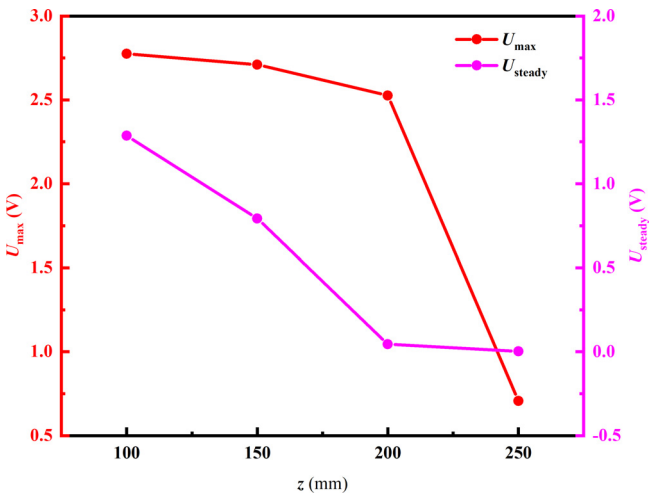

FIG. 18. The effect of arrangement depth on the maximum voltage and steady voltage (T_{op} = 565 °C, h = 50 mm).

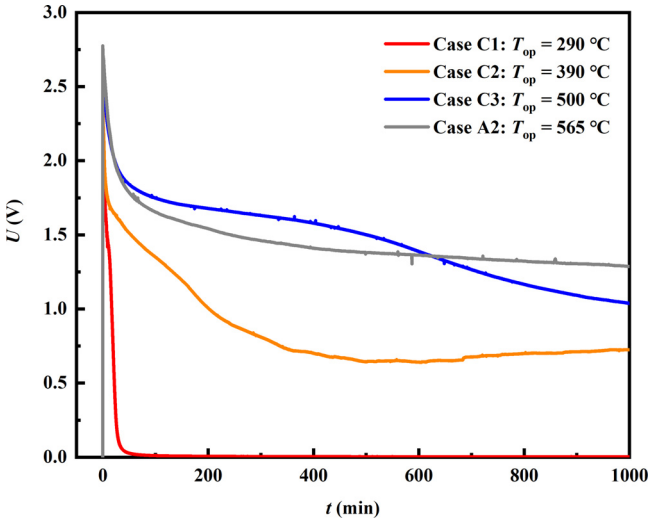

FIG. 19. Voltage evolution of the measuring point at different operating temperatures ($h = 50$, $z = 100$ mm).

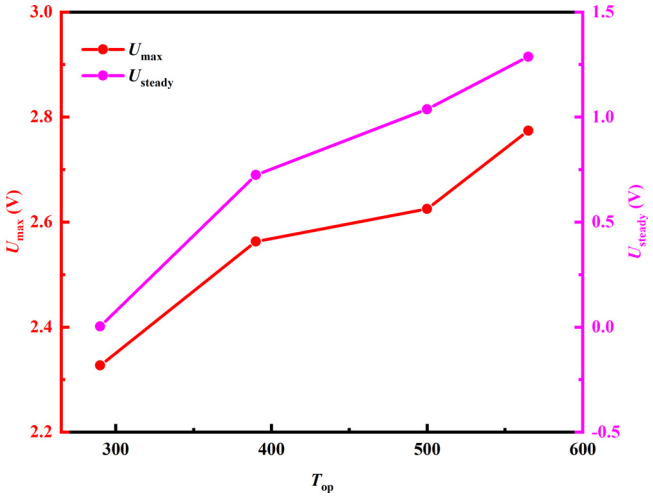

FIG. 20. The effect of operating temperature on the maximum voltage and steady voltage ($h = 50$, $z = 100$ mm).

CSP plant, timely circuit detection signal processing and prompt mechanisms are required to ensure that the leakage accident is not missed.

V. CONCLUSIONS

Molten salt tank leak detection technology is critical for the timely detection and treatment of leaks. However, the current thermocouple leak detection methods cannot meet these needs, and there is an urgent need for a better leak detection method. In this paper, a molten salt tank leakage detection method based on the conductivity of molten salt at high temperatures is proposed for the first time, and a lab-scale tank foundation experimental system is built to verify its feasibility. The results show that the proposed leakage detection method is feasible. In addition, the influences of the vertical spacing, arrangement depth, and operating temperature on the detection effect are studied to optimize the detection circuit. The following conclusions are obtained.

(1) During the leakage process, the temperature of each position contacting with the molten salt presents a trend that first rises quickly, then drops gradually, and finally stabilizes. Since the thermal conductivity of molten salt is better than that of the filler and air, the temperature of the area where the molten salt exists after the molten salt leaks is higher than that before the leakage, and the difference increases with the operating temperature. When the operating temperature increases from 290 to 565 °C, the difference at $z = 50$ mm increases from 1.2 to 6.3 °C.

(2) The maximum migration depth and maximum migration width of molten salt leakage into the fillers increase and decrease with the operating temperature, respectively. When the operating temperature increases from 290 to 565 °C, the maximum migration depth and maximum migration width increase by 97.7% and decrease by 7.5%, respectively.

(3) A model explaining the morphological change of the solid molten salt block (SMSB) is proposed. The shape change of the SMSB under different operating temperatures confirms the reliability of the model. According to the model, the fillers after the molten salt leakage can be divided into the non-solidification zone, main solidification zone, second solidification zone, and no molten salt zone. After the molten salt leaks, the SMSB will be formed in the main solidification zone or in the main solidification zone and the second solidification zone.

(4) The proposed molten salt tank leakage detection method has good feasibility. When the molten salt leakage is detected, the voltage of the constant resistor rises first, then drops, and finally reaches a steady value. The vertical spacing, arrangement depth, and operating temperature have significant influences on the detection effect. To achieve rapid and continuous detection of leakage accidents of molten salt tanks, the vertical spacing should be less than 50 mm, and the arrangement depth should be as close as possible to the bottom of the molten salt tank, preferably within 150 mm. The low operating temperature is not conducive to the detection effect. When the detection circuit is used in the cold tank of the CSP plant, timely circuit detection signal processing and prompt mechanisms are required to ensure that the leakage accident is not missed.

ACKNOWLEDGMENTS

The project is supported by the National Natural Science Foundation of China (No. 52036008).

AUTHOR DECLARATIONS

Conflict of Interest

The authors have no conflicts to disclose.

Author Contributions

Yuhang Zuo: Conceptualization (lead); Data curation (lead); Investigation (lead); Methodology (lead); Visualization (lead); Writing – original draft (lead); Writing – review and editing (lead). **Zhonghua Huang:** Conceptualization (equal); Investigation (equal); Methodology

(equal). **Hui Zhao:** Conceptualization (equal); Investigation (equal); Methodology (equal). **Mingrui Zhang:** Investigation (equal). **Fangzheng Cheng:** Investigation (equal). **Hua Shi:** Investigation (supporting). **Hao Zhou:** Conceptualization (equal); Funding acquisition (lead); Methodology (equal); Project administration (lead); Resources (lead); Supervision (lead); Writing – review and editing (equal).

DATA AVAILABILITY

The data that support the findings of this study are available from the corresponding author upon reasonable request.

REFERENCES

[1]U. Pelay, L. Luo, Y. Fan, D. Stitou, and M. Rood, Renewable Sustainable Energy Rev. **79**, 82 (2017).
[2]A. Bonk, S. Sau, N. Uranga, M. Hernaiz, and T. Bauer, Prog. Energy Combust. Sci. **67**, 69 (2018).
[3]H. Zhou, Y. Zuo, M. Zhou, and Y. Li, J. Renewable Sustainable Energy **13**, 023704 (2021).
[4]Z. Wan, J. Wei, M. A. Qaisrani, J. Fang, and N. Tu, Appl. Therm. Eng. **167**, 114775 (2020).
[5]Y. Li, X. Xu, X. Wang, P. Li, Q. Hao, and B. Xiao, Sol. Energy **152**, 57 (2017).
[6]Y. Tian and C. Y. Zhao, Appl. Energy **104**, 538 (2013).
[7]T. Bauer, N. Pfleger, D. Laing, W. D. Steinmann, M. Eck, and S. Kaesche, *High-Temperature Molten Salts for Solar Power Application* (Elsevier, 2013).
[8]F. Manenti and Z. Ravaghi-Ardebili, Energy **55**, 89 (2013).
[9]X. Li, E. Xu, S. Song, X. Wang, and G. Yuan, Renewable Energy **113**, 1311 (2017).
[10]Q. Yu, X. Li, Z. Wang, and Q. Zhang, Energy **198**, 117183 (2020).
[11]G. Peiró, J. Gasia, L. Miró, C. Prieto, and L. F. Cabeza, Appl. Energy **178**, 394 (2016).
[12]F. Zaversky, J. García-Barberena, M. Sánchez, and D. Astrain, Sol. Energy **93**, 294 (2013).
[13]C. Suárez, A. Iranzo, F. J. Pino, and J. Guerra, Appl. Energy **142**, 56 (2015).
[14]A. K. A. Araújo and G. I. Medina T, Sol. Energy **176**, 358 (2018).
[15]S. Relloso and E. Delgado, paper presented at the SolarPaces 2009 Conference, Berlin, Germany (2009), pp. 1–9.
[16]C. Prieto, L. Miró, G. Peiró, E. Oró, A. Gil, and L. F. Cabeza, Sol. Energy **135**, 518 (2016).
[17]H. Zhou, H. Shi, Y. Zhu, and W. Fang, J. Renewable Sustainable Energy **12**, 14101 (2020).
[18]H. Price, M. Mehos, D. Kearney, R. Cable, B. Kelly, G. Kolb, and F. Morse, "Concentrating solar power best practices study," NREL Report No. TP-550-75763 (Woodhead Publishing, 2021).
[19]S. H. Gage, D. Kesseli, J. Dupree, C. Kimbal, J. Rigby, J. Yates, B. Morrison, G. Bigham, and C. S. Turchi, Sol. Energy Mater. Sol. Cells **226**, 111099 (2021).
[20]G. Wang, S. Yu, S. Niu, Z. Chen, and P. Hu, Appl. Therm. Eng. **170**, 115010 (2020).
[21]H. Zhou, H. Shi, Z. Lai, Y. Zuo, S. Hu, and M. Zhou, Appl. Therm. Eng. **170**, 114968 (2020).
[22]M. Song and R. Viskanta, Int. J. Heat Mass Transfer **44**, 733 (2001).
[23]N. Weisbrod, M. R. Niemet, M. L. Rockhold, T. McGinnis, and J. S. Selker, J. Contam. Hydrol. **72**, 109 (2004).
[24]R. Hird and M. D. Bolton, Proc. R. Soc. A **472**, 20150710 (2016).
[25]M. Dawson, D. Borman, R. B. Hammond, D. Lesnic, and D. Rhodes, Comput. Chem. Eng. **71**, 331 (2014).
[26]J. Shan, J. Ding, and J. Lu, Energy Procedia **69**, 2072 (2015).
[27]J. Wu, J. Ding, J. Lu, and W. Wang, Int. J. Heat Mass Transfer **111**, 312 (2017).
[28]Y. Zhang, J. Wu, W. Wang, J. Ding, and J. Lu, Int. J. Heat Mass Transfer **129**, 397 (2019).
[29]C. Ling, A. Revil, F. Abdulsamad, Y. Qi, A. Soueid Ahmed, P. Shi, S. Nicaise, and L. Peyras, J. Hydrol. **572**, 51 (2019).
[30]T. K. Chan, C. S. Chin, and X. Zhong, IEEE Access **6**, 78846 (2019).
[31]A. F. Colombo, P. Lee, and B. W. Karney, J. Hydro-Environ. Res. **2**, 212 (2009).
[32]N. Hafizha Musthafa, B. Hooi, Y. Kwang, and H. M. Fa dzil, Adv. Sci. Lett. **23**, 10777 (2017).
[33]J. Bonilla, M. M. Rodríguez-García, L. Roca, A. de la Calle, and L. Valenzuela, Energy **152**, 840 (2018).
[34]J. K. Carson, S. J. Lovatt, D. J. Tanner, and A. C. Cleland, Int. J. Heat Mass Transfer **48**, 2150 (2005).